

PIV Flow Field Measurements in a Rotating U-Shaped Channel. Comparison of smooth and 90° rib-roughened walls.

Yves SERVOUZE, Christophe BROSSARD and Pierre GICQUEL

DEFA

Office National d'Etudes et de Recherches Aéronautiques

BP 72 – 29 avenue de la Division Leclerc 92322 Châtillon Cedex, FRANCE

Phone: +33 1 69 93 60 13, Fax: +33 1 69 93 61 62, E-mail: Yves.Servouze@onera.fr

ABSTRACT

This paper presents our latest efforts in an ongoing program to improve the understanding of aerodynamic and thermal phenomena of internal blade cooling by forced convection and to incorporate this knowledge into predictive tools. The particular objectives of this program are to estimate the use of the 2D Particle Image Velocimetry technique and to produce experimental data obtained for various boundary conditions in order to anchor a computer code being developed in parallel.

In this paper we compare the results of the investigations of the flow in two different configurations of the channel : 1) smooth internal walls, 2) internal walls of only one branch equipped with square profile ribs inclined at 90° to the main flow and placed on opposite walls (trailing and leading surfaces when in rotation). The test channel which consists in two radial branches connected by a 180° bend, rotates in orthogonal mode. The experimental conditions tested are : Rotation number (Ro) of 0 and 0.33 for Reynolds number (Re) of 5000 and Rotation number of 0 and 0.066 for Reynolds number of 25000.

PIV measurements reveal the presence of vortices and separation bubbles due to the bend and the ribs in the stationary case. With rotation, the arrangement of the flow is different : **In the centrifugal branch**, it is characterized by a shift of maximum axial velocity toward the trailing edge which is consistent with the enhancement of the convective heat transfer observed along this wall. **In the centripetal branch**, the secondary flow which results of added effects of bend and rotation consists in a single vortex; we can also observe that the effect of the bend is dominant in this branch. Around ribs, measurements reveal flow contraction/expansion, impingements and separation bubbles.

The largest number of measurements obtained compared to the one previously obtained by Laser Doppler Velocimetry is useful for comparison with numerical calculations.

NOMENCLATURE

B	Buoyancy number, $(\omega r / U) (\omega D_h / U) ((T_{int} - T_{bulk}) / T_{int})$
e	rib height
$2e/D_h$	blockage ratio of ribs
D_h	hydraulic diameter
h	internal convection coefficient
k	thermal conductivity of air
L/D_h	flow length in terms of hydraulic diameter
Nu	Nusselt number, hD_h/k
Nu_o	fully-developed, non-rotating Nusselt number from Dittus-Boelter correlation
Nu/Nu_o	ratio of rotating-to-stationary Nusselt numbers
p/e	pitch-to-height ratio of rib spacing
r	distance from axis of rotation, direction x

Re	Reynolds number, $\rho U D_h / \mu$
Ro	Rotation number, $\omega D_h / U$
s	distance coordinate along the internal wall
T_{bulk}	bulk-averaged temperature of air
T_{int}	internal surface temperature of channel
U	bulk-averaged velocity of main flow
u, v, w	x -, y - and z -components of velocity
u_{inlet}	channel inlet-averaged velocity
x, y, z	orthogonal coordinates
α	angle of ribs relative to channel axis
μ	dynamic viscosity of air
ρ	density of air
ω	rotational velocity of test channel

INTRODUCTION

In order to achieve higher fuel efficiency of gas turbine engines, the hot section and the turbine in particular, is required to operate with high inlet temperatures. This hot gas temperature is increased but at the risk of jeopardizing the mechanical integrity of the turbine blades. Often active cooling of the blades becomes necessary with one common technique being that of internal forced convection. Designers of such a cooling circuit must have an understanding of the physical mechanisms at play as well as accurate predictive tools in order to design a system that cools the blade while minimizing the required air flow.

This paper summarizes a recent research effort which addresses flow field measurements through a rotating, U-shaped channel whose internal surfaces are successively smooth and furnished with ribs oriented at $\alpha = 90^\circ$ to the bulk flow. This experimental program employs 2D Particle Image Velocimetry to map velocity fields. We can note significant improvement over the 3D Laser Doppler Velocimetry technique used in the past Servouze (1999).

It should be noted that this effort is part of a larger initiative to generate experimental data (convective heat transfer coefficient and map velocity fields) in order to support code development being conducted in parallel. As such, the results presented here are not an attempt to examine a real blade design but rather an examination of a simplified yet applicable geometry to be used in code validation. The goal is to improve the understanding and predictive tools (CFD codes) for turbine blade cooling designers

REVIEW OF PHYSICAL MECHANISMS

An internal flow passage of a gas engine turbine blade is modeled by a constant cross-section, U-shaped channel (Fig. 1) which is composed of a radial outflow segment (centrifugal

branch), a 180° bend and a radial inflow segment (centripetal branch). The convection coefficient profile around the internal perimeter and along the channel is strongly influenced by the secondary flows present in the two branches.

Two of the main mechanisms responsible for secondary flows are due to rotation – Coriolis and buoyancy forces – while a third arises from the geometry of the channel: shape, bend, ribs. The hydrodynamic characteristics and the consequential effects on heat transfer of these mechanisms are presented briefly.

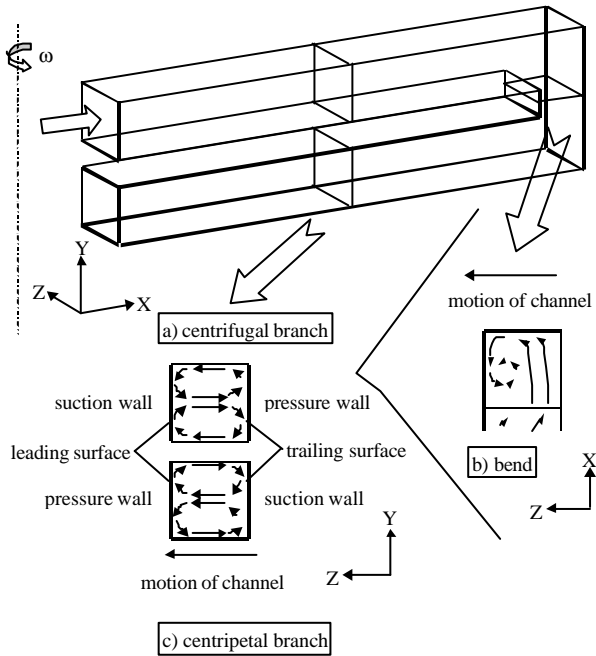


Fig.1 Simplified model of blade internal cooling passage. Rotating, smooth-walled channel with cross-section showing Coriolis-induced secondary flow.

Outward Branch. (Fig 1a) Qualitatively, Coriolis force induces a secondary flow which consists in two symmetric vortices. This secondary flow distorts the velocity and temperature radial profiles; thus the friction factor and heat transfer coefficient h are modified.

Along the trailing wall where the fluid impinges (Fig 1a), the heat transfer coefficient is greater than the value for the equivalent stationary case; 2.5 – 3.0 times the non-rotating value according to the experiments of Han (1994). This comparison is often expressed in terms of Nusselt number ($Nu = hD_h/k$) normalized by the stationary value, Nu_o , given by the standard Dittus-Boelter relation. Bons (1997) observed $Nu/Nu_o = 2.2$ at an axial location of $x/D_h = 8$. The rotating-to-stationary Nu ratio on the trailing surface increases as a function of the non-dimensional Rotation number, defined as $Ro = \omega D_h / U$, which represents the ratio of Coriolis to inertial forces. Hwang (1994) found Nu/Nu_o to increase monotonically with increasing Ro yet to diminish with increasing Reynolds number ($Re = \rho U D_h / \mu$). Guidez (1989) showed the same Nu/Nu_o tendencies with regards to Ro and Re .

Rotation has a negative influence on the leading wall where the Nusselt number falls below the stationary channel value (for equivalent Reynolds number). Guidez (1989) calculated Nu/Nu_o less than unity; Han (1994) found the ratio to be as low as 0.4. The leading wall does not benefit from an impingement of fluid as does the trailing wall (Fig 1a)

Bend. (Fig 1b) The added effects of rotation and geometry of the bend, result in a secondary flow which consists in a dominant single vortex located close to the leading wall. However, for a low

Rotation number Ro a small vortex can appear in the corner of the trailing and the out walls as observed by Liou (2002). A heat transfer coefficient enhancement is observed on the leading and out walls, in accordance with the impingement of fluid.

Inward Branch. (Fig 1c) In the centripetal branch without bend located upstream, the direction of the Coriolis force is reversed, then the secondary flow has similar two symmetric vortices which rotates in the inverse directions. So, augmentation of the heat transfer coefficient h takes place on the leading wall due to the inverse direction of the Coriolis force. Hwang (1994) measured lower temperatures on the leading wall as compared to the trailing wall and Mochizuki (1994) reported higher Nu on the leading wall.

In the centripetal branch with bend located upstream, the tendency of Nu/Nu_o for inward flow is not as well established as in the centrifugal branch due to the secondary motions generated in the bend. Experimentally, it is difficult to isolate the rotation effects from the bend effects since the latter persist for several diameters along the inward flow and tend to dominate the heat transfer. There is, however, general agreement in the literature that $Nu/Nu_o = 1$ for all walls in the centripetal branch.

Ribs. Ribs placed along the channel walls are also responsible for creating secondary motions. The influence of ribs in a stationary channel is to increase the heat transfer on all walls in comparison to a (stationary) smooth-walled channel. The circulation acts to move the warmer air away from the walls to mix with the cooler bulk. Han [13] calculated enhancements of 70 – 150% on the ribbed walls and 10 – 40% on the smooth side walls due to the presence of ribs.

Ribs also increase the effective surface area available for heat transfer. Taslim (1997) estimated heat transfer from the rib surfaces could account for as much as 55% of the total in a channel with two ribbed walls while Çakan (2000) calculated an 8% contribution in the case of one ribbed wall.

EXPERIMENTAL METHODS

For velocity field measurements, data is obtained in an unheated accessible channel. In these conditions the Buoyancy number $B = 0$. While it is acknowledged that velocity field measurements made under such adiabatic conditions do not include the effects of buoyancy-induced secondary motion, valuable insight may still be gained measuring the secondary flow fields attributed to the Coriolis force and angled ribs.

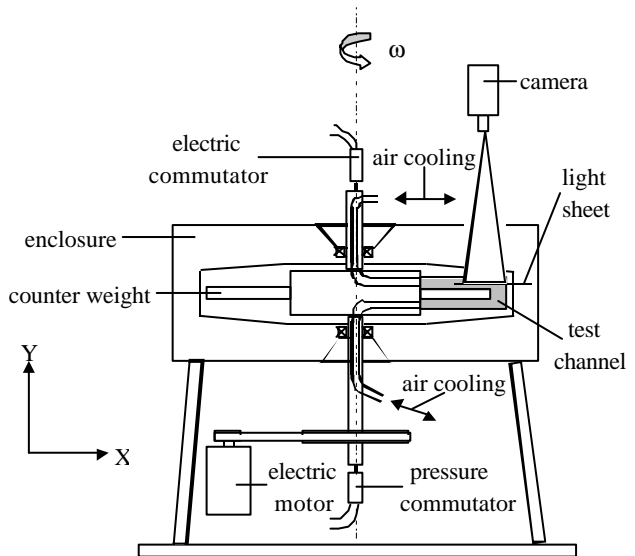


Fig. 2 Sketch of the experimental rig.

Experimental rig

The experimental rig which is shown on Fig 2, allows thermal and aerodynamic measurements on two different models, with the same geometry. It has been described already by Servouze (1998), (1999).

The model (Fig 3), connected to a support arm (at $r = 220.5$ mm) which contains two passages for the arriving and departing air flow, rotates within an enclosure. Air at 1 bar and 280 K (measured far upstream of the test channel) enters the branch of the channel after passing through a straight radial passage having the same cross-section and a honeycomb flow straightener (located $4D_h$ upstream of the branch inlet). This passage which is part of the support, is connected to a vertical circular duct included in the shaft. As anemometry measurements are made inside the upper arm of the test channel model, the cooling air inlet, which is located either at the lower or the upper part of the rotating shaft, allows to observe the flow in either the centrifugal or in the centripetal branch.. Mass flow is controlled with a sonic hole, its temperature and its pressure are measured at the inlet and the outlet of the model. An electric commutator (for thermocouples) and a pressure commutator ensure the connection between rotating and static parts. The rotating parts are driven by a controlled electric motor via a toothed pulley. For PIV measurements, the maximum rotating speed $\omega = 110$ rd/s (=1000 rpm). Control parameters are sent to a data acquisition system connected to a minicomputer PC, for storage and analysis.

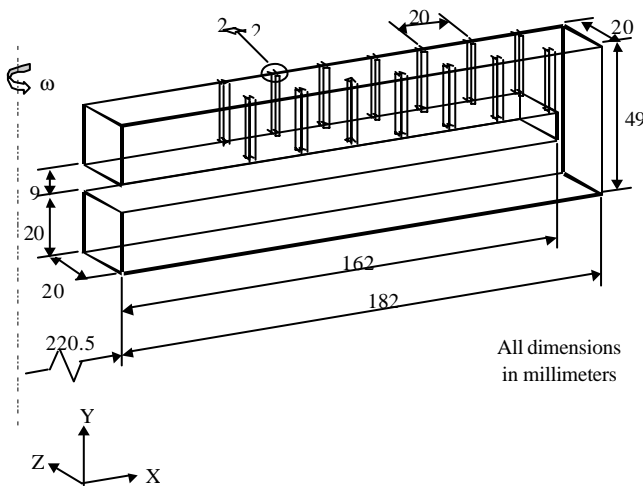


Fig. 3 Geometry of the experimental U-shaped channel for aerodynamic tests.

Test Channels

Experiments are conducted using the U-shaped channel depicted in Fig 3. Each branch and the bend have a constant square cross-section (20 x 20 mm, $D_h = 20$ mm). Each branch measures 162 mm from the inlet to beginning of bend. The thickness of the separation walls is 9 mm.

To perform the tests with ribs, two opposite internal walls of the upper branch are roughened with inline ribs in a parallel configuration oriented at $\alpha = 90^\circ$ relative to the channel axis. The ribs have square profiles (2 x 2 mm) yielding a blockage ratio of $2e/D_h = 0.2$. There are seven pairs spaced along the side-walls with a pitch-to-height ratio of $p/e = 10$. In rotation, the ribbed surfaces are the leading and trailing walls.

For flow field measurements two non-parallel walls (upper and lateral) of the upper branch are made of glass to permit optical access. In this case, ribs on the lateral wall are made of glass and glued onto the wall maintaining the same blockage ratio, pitch-to-height ratio and cross-section.

Flow Field Measurements

A 2-D Particle Image Velocimetry system is used to measure the flow field in horizontal planes inside the upper branch. The PIV system is chosen in order to obtain a high density of velocity measurements.

This technique (Fig. 4) employs two horizontal planar pulses of light (with controlled time interval) which pass through the glass side-wall of the channel illuminating the micron-sized oil droplets suspended in the air flow. Through the upper glass wall, a CCD camera captures these two images which are treated by special software in order to calculate an “instantaneous” velocity map based on the particle displacements observed between the two images and the known time interval. This process is repeated at least one hundred times in order to calculate an average velocity field for the given measurement plane, the results of which are presented in this paper. Due to geometry constraints, only measurement planes parallel to the upper and lower walls of the channel are investigated to obtain the u - and w -components of velocity.

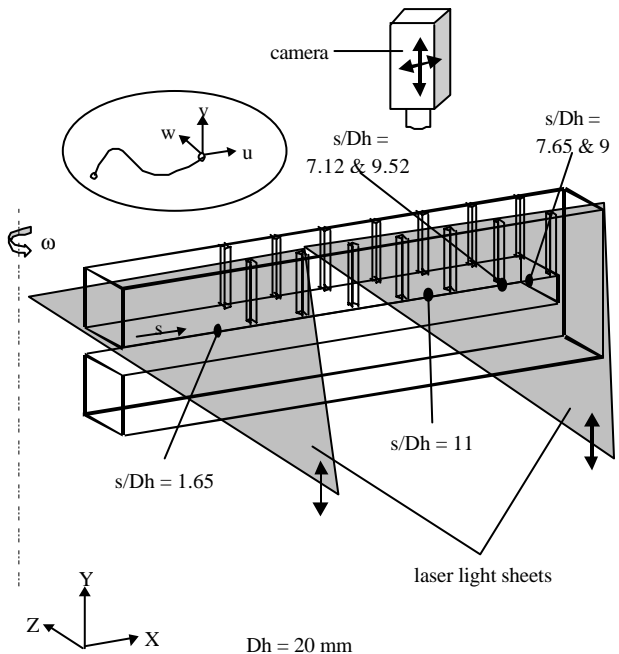


Fig. 4 Experimental arrangement for P.I.V. measurements.

The advantages realized by PIV include a very short data acquisition time and a high resolution of measurements (one millimeter spacing in the transversal and axial directions). The vertical separation between measurement planes is also one millimeter. Velocity fields are determined for static and rotating modes, the latter requiring a trigger mechanism to synchronize the laser and camera operations with the channel passage. For this mode, the tangential component of velocity (w -component) sensed by the camera but due to the motion of the channel is subtracted from the measurements. This component is the product of angular velocity and local radius.

Experimental Conditions

Velocity field tests for both smooth and 90° rib-roughened walls, were conducted at Rotation numbers of $Ro = 0$ & 0.066 for $Re = 25000$ and $Ro = 0$ & 0.33 for $Re = 5000$.

RESULTS AND DISCUSSION

In this paragraph we examine successively:

- General views of the flow development (u and w components) in the planes $y/Dh = 0.05$ & 0.45 .
- Detailed plots of streamwise velocity (u) and secondary velocity (w) at various cross sections s/Dh of the plane $y/Dh = 0.45$.

Flow Development – Outward Branch of Smooth Channel:

Figure 5 presents three velocity fields in the outward branch. In these images, flow for $Re = 5000$ is from left to right with the start of the bend indicated by the transverse line.

For the stationary case $Ro = 0$ (Fig. 5a), flow in the plane $y/Dh = 0.45$ is established. The velocity profile corresponds to a turbulent flow.

In the rotating case $Ro = 0.33$, comparing flow in the plane $y/Dh = 0.45$ (Fig. 5b) and in the plane $y/Dh = 0.05$ closed to the lower wall (Fig. 5c), we observe that velocity vectors are oriented toward the trailing wall in the first plane and toward the leading wall in the second plane. This is consistent with the secondary flow (see Fig. 1a) resulting from the Coriolis force. Moreover, in the two planes we can observe that the u -component is greater close to the trailing wall. At the bend, the classical vortex is established.

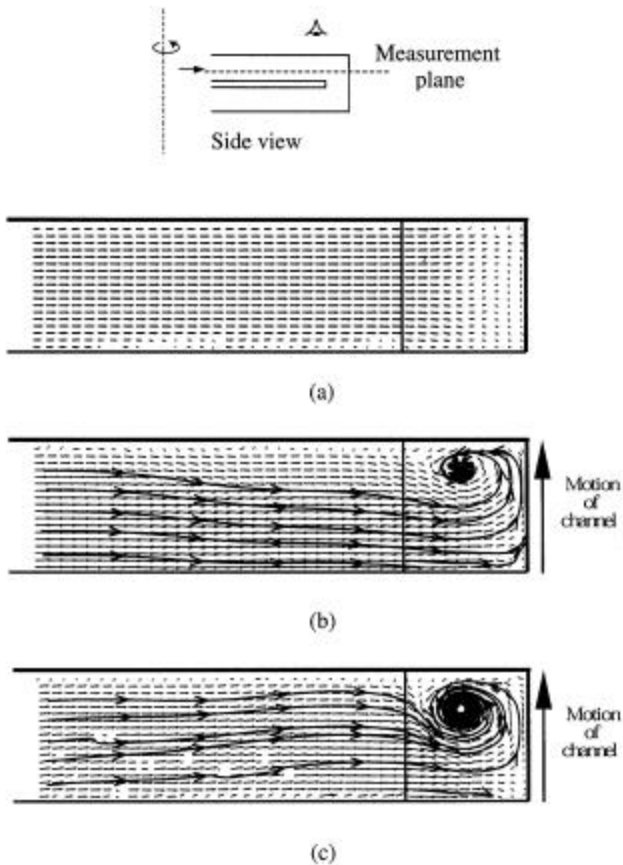


Fig. 5 Flow development in horizontal planes – Outward branch of smooth channel.

- (a) $Re = 5000, Ro = 0$, plane $y/Dh = 0.45$
- (b) $Re = 5000, Ro = 0.33$, plane $y/Dh = 0.45$
- (c) $Re = 5000, Ro = 0.33$, plane $y/Dh = 0.05$

Flow Development – Inward Branch of Smooth Channel

Figure 6 presents three velocity fields in the inward branch. In these images, flow for $Re = 5000$ is from right to left with the end of the bend indicated by the transverse line.

For the stationary case $Ro = 0$ (Fig. 6a), flow in the plane $y/Dh = 0.05$ is characterized by two counter-rotating vortices generated as the flow negotiates the 180° turn. A separation bubble is detected, it staggers on a distance of $1xDh$ just downstream of the bend. Farther downstream, the flow is symmetric.

In the rotating case $Ro = 0.33$, the flow in the plane $y/Dh = 0.05$ (Fig. 6b), the secondary motion generated in the bend is coupled with the Coriolis-induced motion to create a single, large vortex exiting the bend; a asymmetrical separation bubble is observed on the lower wall. Farther downstream, velocity vectors are oriented toward the trailing wall. This asymmetry is consistent with the observed augmentation of leading wall heat transfer.

In the rotating case $Ro = 0.33$, the flow in the plane $y/Dh = 0.45$ (Fig. 6c) shows that the vortex into the bend and the separation bubble have disappeared. As for the other plane, farther downstream, velocity vectors are oriented toward the trailing wall.

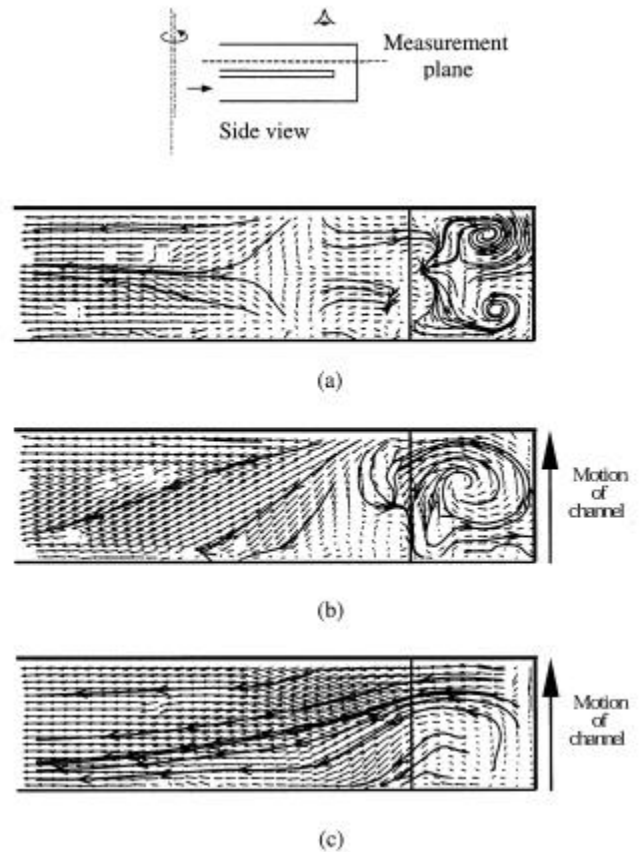


Fig. 6 Flow development in horizontal planes – Inward branch of smooth channel.

- (a) $Re = 5000, Ro = 0$, plane $y/Dh = 0.05$
- (b) $Re = 5000, Ro = 0.33$, plane $y/Dh = 0.05$
- (c) $Re = 5000, Ro = 0.33$, plane $y/Dh = 0.45$

Flow Development – Outward Ribbed Branch

Figure 7 presents three velocity fields in the outward branch. In these images, flow for $Re = 5000$ is from left to right with the start of the bend indicated by the transverse line. For the stationary case $Ro = 0$ (Fig. 7a), flow in the plane $y/Dh = 0.45$ is periodic and symmetric upstream of the bend. A more detailed inspection than presented here reveals flow deflection, impingement and reversal in the vicinity of the ribs. At the bend, two classical counter-rotating vortices begin to appear. In the rotating case $Ro = 0.33$, comparing flow in the plane $y/Dh = 0.45$ (Fig. 7b) and in the plane $y/Dh = 0.05$ closed to the lower wall (Fig. 7c), the comments made for the outward smooth branch are always relevant.

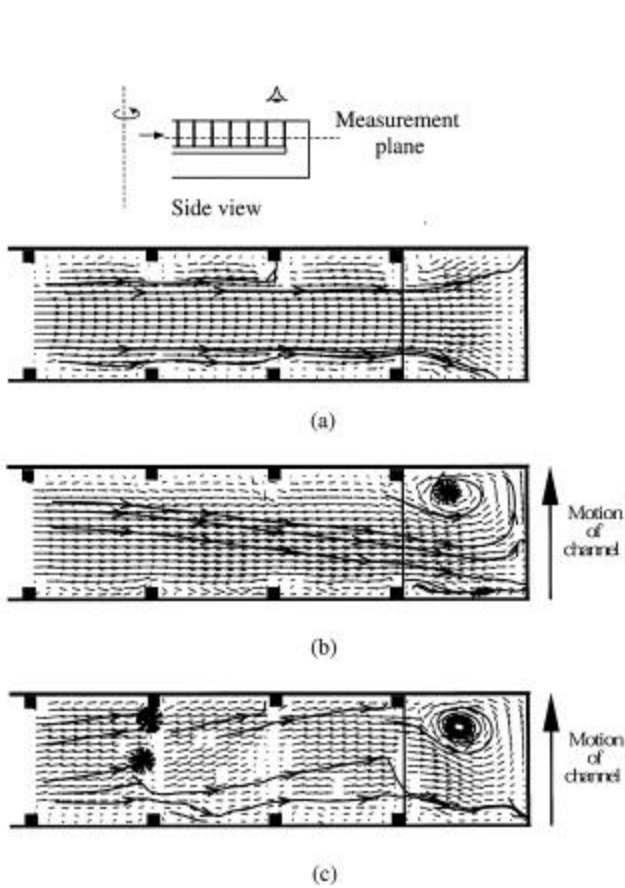


Fig. 7 Flow development in horizontal planes – Outward ribbed branch.

- (a) $Re = 5000, Ro = 0, \text{ plane } y/Dh = 0.45$
- (b) $Re = 5000, Ro = 0.33, \text{ plane } y/Dh = 0.45$
- (c) $Re = 5000, Ro = 0.33, \text{ plane } y/Dh = 0.05$

Flow Development – Inward Ribbed Branch

Figure 8 presents three velocity fields in the inward branch. In these images, flow for $Re = 5000$ is from right to left with the end of the bend indicated by the transverse line. For the stationary case $Ro = 0$ (Fig. 8a), as observed inside the smooth channel, flow in the plane $y/Dh = 0.05$ reveals two counter-rotating vortices generated as the flow negotiates the 180° turn. Farther downstream, the flow is fairly symmetrical. No separation bubble is detected just downstream of the bend, as is the case for the stationary smooth-walled channel. On the other hand reversal are observed just behind the first ribs.

In the rotating case $Ro = 0.33$, measurements made in the plane $y/Dh = 0.05$ (Fig. 8b) reveal the large vortex exiting the bend. Yet, a small vortex appears closed to the trailing wall. Downstream, no separation bubble is observed on the lower wall, it is replaced by a dead area where the flow moves from the leading toward the trailing wall. Farther downstream, velocity vectors are oriented toward the trailing wall. In the rotating case $Ro = 0.33$ and in the plane $y/Dh = 0.45$ (Fig. 8b) it seems downstream of the bend, that the effects of rotation are less pronounced.

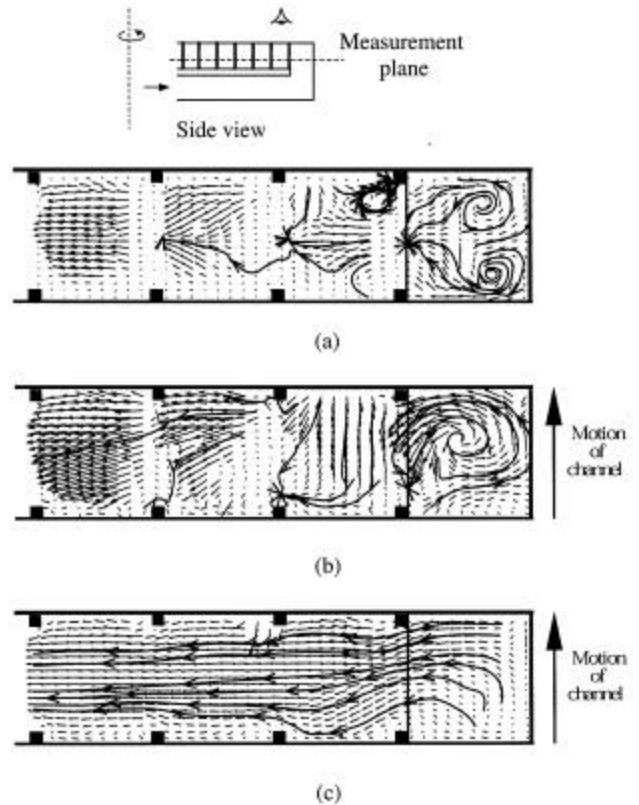


Fig. 8 Flow development in horizontal planes – Inward ribbed branch.

- (a) $Re = 5000, Ro = 0, \text{ plane } y/Dh = 0.05$
- (b) $Re = 5000, Ro = 0.33, \text{ plane } y/Dh = 0.05$
- (c) $Re = 5000, Ro = 0.33, \text{ plane } y/Dh = 0.45$

Flow Development – Inward Branch – $Re = 25000$

Figure 9 which presents three velocity fields for $Re = 25000$ in the inward branch (smooth and ribbed wall) allows to comment the effect of Reynolds number. For the stationary case $Ro = 0$ (Fig. 9a), the major difference lies in the extent of the separation bubble which is about $1.5xDh$ ($1xDh$ for $Re = 5000$). In the rotating case (plane $y/Dh = 0.05$ - Fig. 9b & Fig. 9c) we observe that the effect of rotation is less pronounced as the Rotation number $Ro = 0.066$ is lower and the Reynolds number $Re = 25000$ is higher. This is clear at the bend where the two counter-rotating vortices are present in place of the single vortex; however the structure is asymmetric. Farther downstream, the separation bubble is always detected in both cases. The asymmetrical flow is the result of rotation.

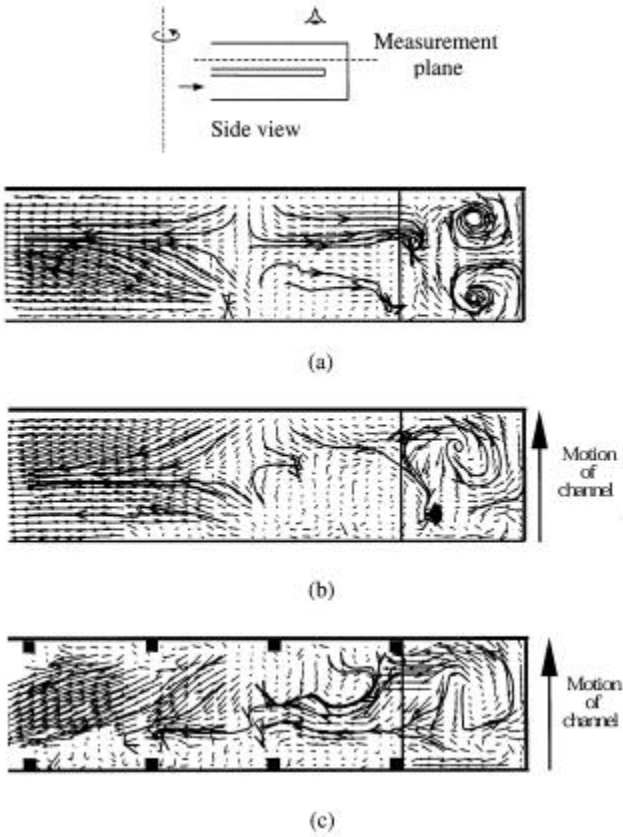


Fig. 9 Flow development in horizontal planes – Intward branch.
 (a) Smooth channel, $Re = 25000$, $Ro = 0$, plane $y/Dh = 0.05$
 (b) Smooth channel, $Re = 25000$, $Ro = 0.066$, plane $y/Dh = 0.05$
 (c) Ribbed walls, $Re = 25000$, $Ro = 0.066$, plane $y/Dh = 0.05$

Detailed Plots – Smooth-walled Channel – $Re = 5000$

Figures 10 & 11 show $u(z)$ and $w(z)$ data for the stationary case $Ro = 0$. In the outward branch $s/Dh = 1.65$ & 7.65 we observe the boundary layer development and core acceleration ($u(z)$). The $w(z)$ data show no significant transverse component. In the inward branch $s/Dh = 9$ & 11 $u(z)$ and $w(z)$ data show the effect of the 180° turn. A cross-stream mean velocity as high as 1.4 times inlet mean velocity is observed (u/u_{inlet}), it is the effect of the counterrotating symmetric vortex pair prevailed inside the turn. This effect is also demonstrated by the high transverse component. Farther downstream, the effect decreases.

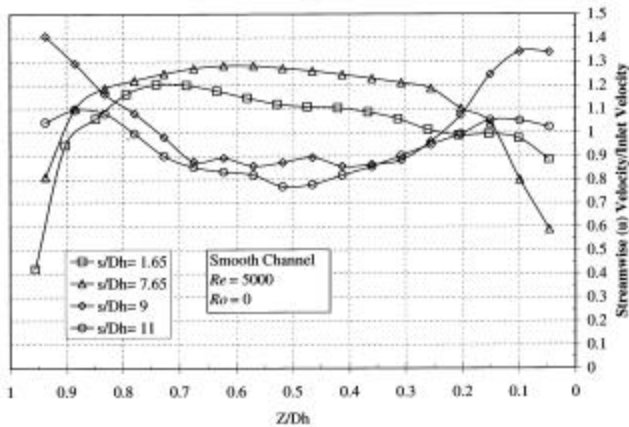


Fig. 10 Smooth channel - Streamwise $u(z)$ velocity profile data in various locations s/Dh of plane $y/Dh = 0.45$, for $Re = 5000$, $Ro = 0$.

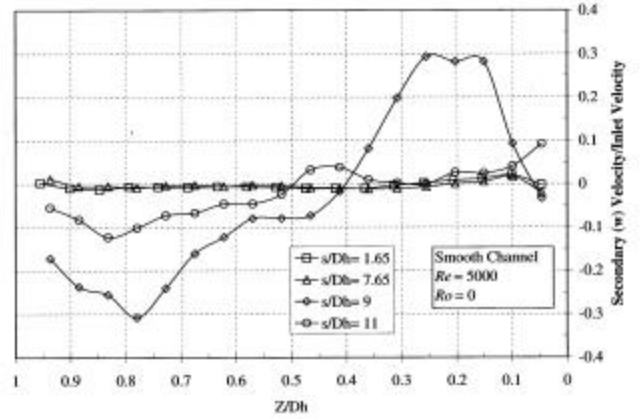


Fig. 11 Smooth channel - Secondary $w(z)$ velocity profile data in various locations s/Dh of plane $y/Dh = 0.45$, for $Re = 5000$, $Ro = 0$.

Figures 12 & 13 show $u(z)$ and $w(z)$ data in the rotating case $Ro = 0.33$. The profile of $u(z)$ is gradually distorted in the outward branch $s/Dh = 1.65$ & 7.65 with a thinner boundary layer closed to the trailing wall. In the inward branch the profiles of $u(z)$ are distorted with a maximum of u -component close to the leading wall, this is clear in the cross-section $s/Dh = 9$ where we observe a minimum and a maximum located symmetrically at $z/Dh = 0.25$ and 0.75 ; this profile becomes quite flat in the cross-section $s/Dh = 11$. Except in the cross-section $s/Dh = 1.65$, the $w(z)$ data are negative, this corresponds to a flow which is deflected toward the trailing wall.

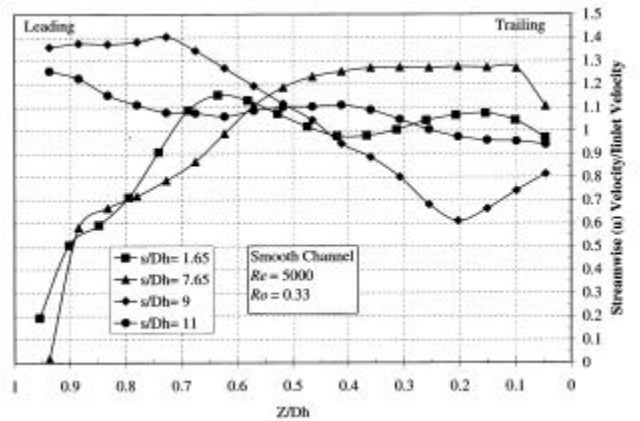


Fig. 12 Smooth channel - Streamwise $u(z)$ velocity profile data in various locations s/Dh of plane $y/Dh = 0.45$, for $Re = 5000$, $Ro = 0.33$.

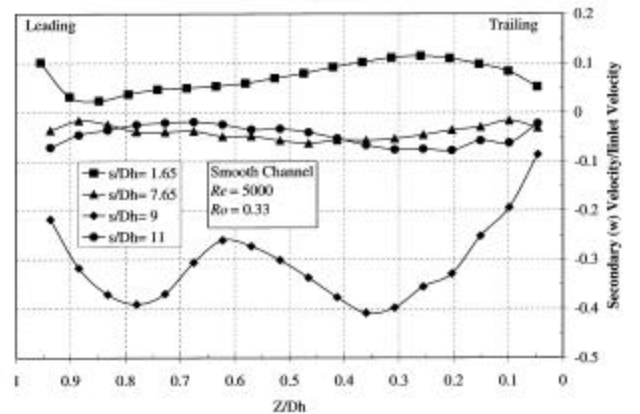


Fig. 13 Smooth channel - Secondary $w(z)$ velocity profile data in various locations s/Dh of plane $y/Dh = 0.45$, for $Re = 5000$, $Ro = 0.33$.

Detailed Plots – Outward Ribbed Branch – $Re = 5000$

Figures 14 & 15 show $u(z)$ and $w(z)$ data obtained in the outward branch for the stationary case $Ro = 0$. In the cross-section $s/Dh = 7.12$ which corresponds to the smallest section of passage for the flow, we observe a core acceleration with a maximum factor of 1.6 for u/u_{inlet} . Downstream, in the cross-section $s/Dh = 7.65$, the profile of $u(z)$ gets the shape of a parabola: this is consistent with the vicinity of the walls where reversed flows take place just behind the ribs (Fig. 14). At the same cross-section, the profile of $w(z)$ has a maximum and a minimum located close to the walls, this corresponds to the expansion of the flow toward the walls (Fig. 15).

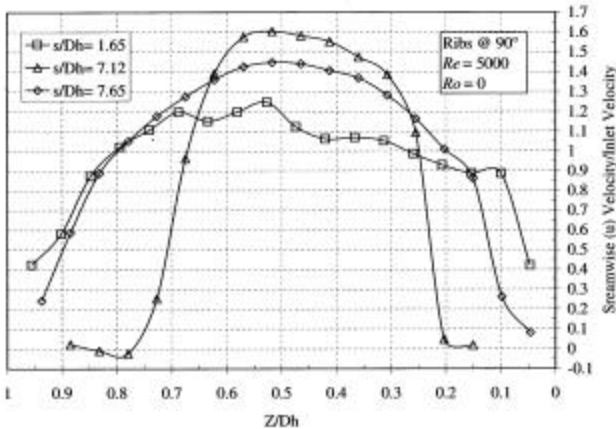


Fig. 14 Outward ribbed branch - Streamwise $u(z)$ velocity profile data in various locations s/Dh of plane $y/Dh = 0.45$, for $Re = 5000$, $Ro = 0$.

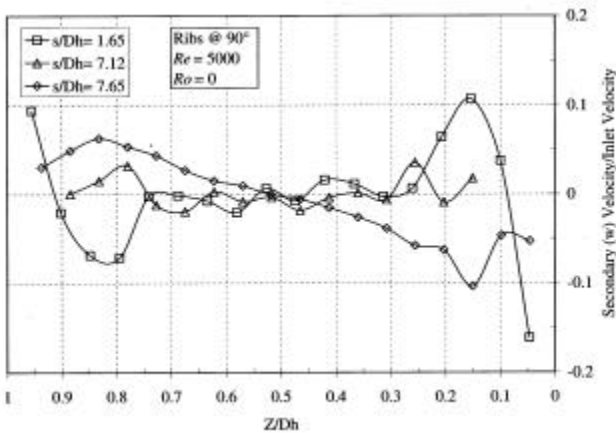


Fig. 15 Outward ribbed branch - Secondary $w(z)$ velocity profile data in various locations s/Dh of plane $y/Dh = 0.45$, for $Re = 5000$, $Ro = 0$.

Figures 16 & 17 show $u(z)$ and $w(z)$ data obtained in the outward branch for the rotating case $Ro = 0.33$. The profiles of $u(z)$ are distorted with a thinner boundary layer close to the trailing edge. In the cross-sections $s/Dh = 7.12$ which corresponds to the smallest section of passage, measurements detect a reversed flow located on the top of the rib at $z/Dh = 0.84$ (Fig. 16). Compared to those obtained in the smooth channel, the profiles of $w(z)$ observed here are quite similar, excepted in the cross-section $s/Dh = 7.12$ where two peaks of negative values of w correspond to the flow-deflection in the vicinity of the ribs (Fig. 17).

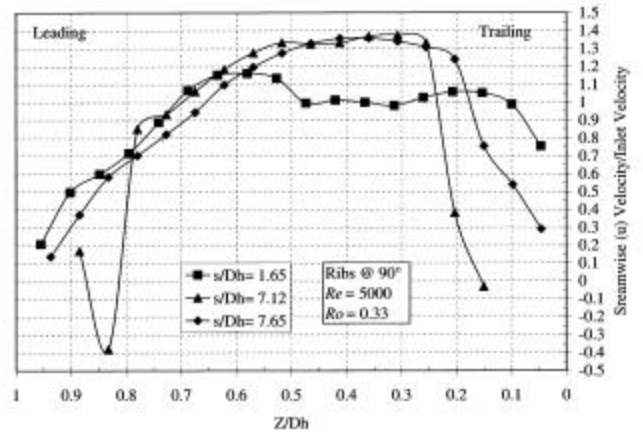


Fig. 16 Outward ribbed branch - Streamwise $u(z)$ velocity profile data in various locations s/Dh of plane $y/Dh = 0.45$, for $Re = 5000$, $Ro = 0.33$.

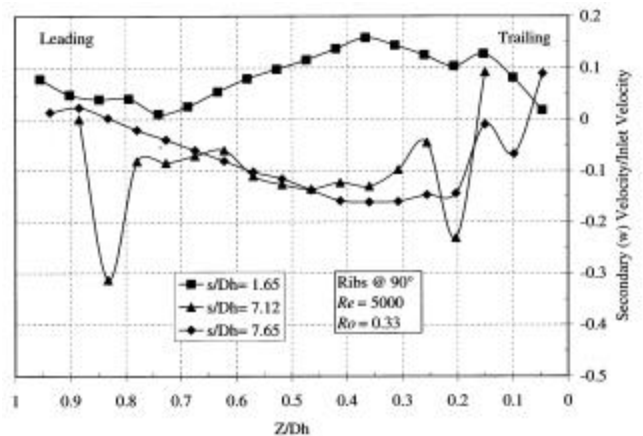


Fig. 17 Outward ribbed branch - Secondary $w(z)$ velocity profile data in various locations s/Dh of plane $y/Dh = 0.45$, for $Re = 5000$, $Ro = 0.33$.

Detailed Plots – Inward Ribbed Branch – $Re = 5000$

Figures 18 & 19 show $u(z)$ and $w(z)$ data obtained in the inward branch for the stationary case $Ro = 0$. Compared to those obtained with the smooth channel, the profiles of $u(z)$ are different with core acceleration and thicker buoyancy layers. The profiles of $w(z)$ in the cross-sections $s/Dh = 9.52$ & 11 allow to suppose that the secondary flow arrangement is greatly dependant of the ribs. Without information about the v -component of the velocity, it is difficult to understand the flow development resulting from the combined effects of bend and ribs.

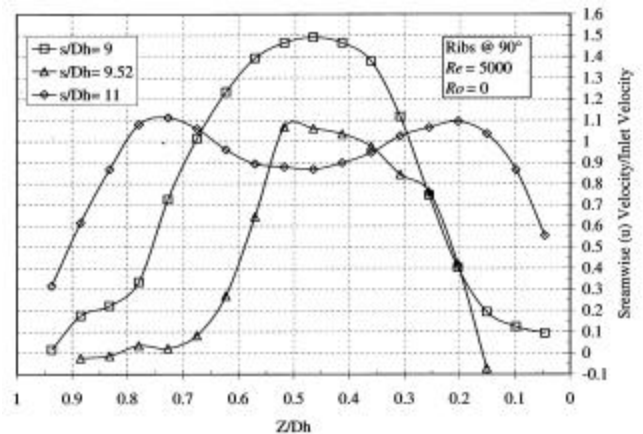


Fig. 18 Inward ribbed branch - Streamwise $u(z)$ velocity profile data in various locations s/Dh of plane $y/Dh = 0.45$, for $Re = 5000$, $Ro = 0$.

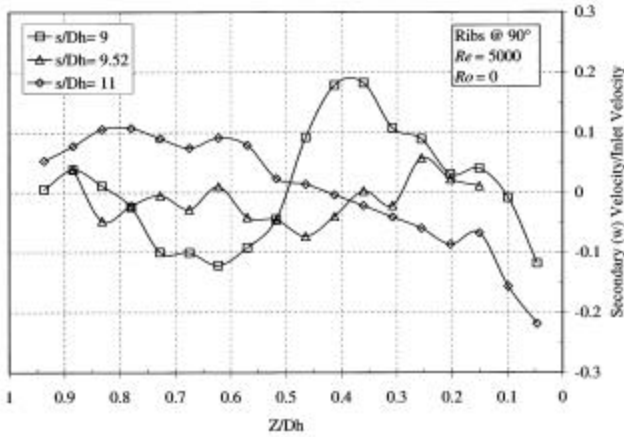


Fig. 19 Inward ribbed branch - Secondary $w(z)$ velocity profile data in various locations s/Dh of plane $y/Dh = 0.45$, for $Re = 5000$, $Ro = 0$.

Figures 20 & 21 show $u(z)$ and $w(z)$ data obtained in the outward branch for the rotating case $Ro = 0.33$. Because of the ribs, the profiles are modified in the vicinity of the walls, but the general shape due to the rotation and observed in the similar case remains.

Because of the limited paper length it is not possible to present data obtained with similar geometries for $Re = 25000$ and $Ro = 0$ & 0.066 . The results show little differences due to a lower effect of rotation.

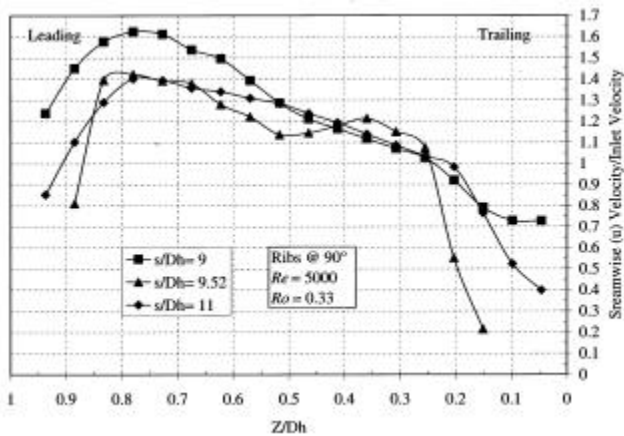


Fig. 20 Inward ribbed branch - Streamwise $u(z)$ velocity profile data in various locations s/Dh of plane $y/Dh = 0.45$, for $Re = 5000$, $Ro = 0.33$.

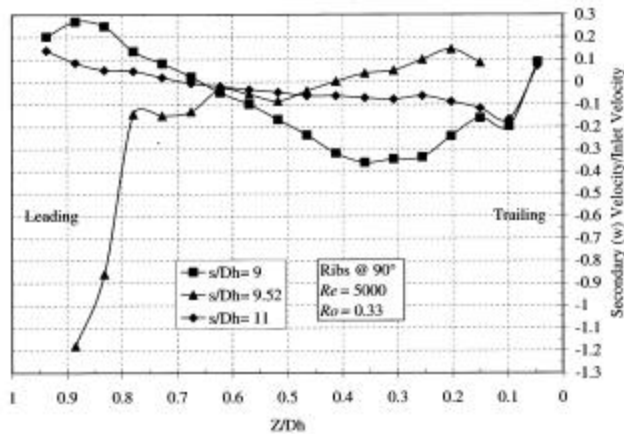


Fig. 21 Inward ribbed branch - Secondary $w(z)$ velocity profile data in various locations s/Dh of plane $y/Dh = 0.45$, for $Re = 5000$, $Ro = 0.33$.

CONCLUSIONS

PIV measurements have been performed in the centrifugal and centripetal branches of a rotating channel having successively internal smooth walls and 90° parallel ribs mounted on the leading and trailing walls. Conclusions drawn from this experimental investigation are summarized below.

1. Rotation of the channel leads to the formation of a secondary flow which creates distorted streamwise velocity profiles consistent with the disparity in heat transfer between the leading and trailing walls. The ribs of the present configuration also create secondary structures that tend to favor local enhancements of heat transfer in their vicinity.
2. In the centrifugal branch, the effect of rotation is clearly demonstrated: velocity vectors are deflected toward the trailing wall, and the streamwise velocity profiles are distorted with the u -component along the trailing wall greater than this along the leading wall.
3. Inside the bend a counterrotating symmetric vortex pair prevails for the stationary case. For the rotating case this secondary structure is replaced by a single vortex with sometimes, depending of the level of the Rotation number Ro and of the presence of ribs, a corner vortex located along the trailing wall.
4. As the secondary flows created by the bend begin to dissipate farther downstream in the centripetal branch, the streamwise velocity profile disparity between the pressure and suction surfaces begins to re-emerge as the vortices associated with the Coriolis forces reform.
5. PIV measurements, despite the fact they are obtained without buoyancy effects, are useful for comparison with computed flow fields. The very short data acquisition time and the high density of measurement points obtained, represent a significant improvement over the LDV technique. Additionally, the successful application of PIV to a rotating measurement field (adjusting for both rotational speed and flowrate) provides a valuable tool for turbine blade cooling research.

ACKNOWLEDGMENTS

The authors express their gratitude to the French Ministry of Defense for their partial financial support of this study as well as for the permission to publish the present results.

REFERENCES

- Bons, J.P., 1997, "Complementary Velocity and Heat Transfer Measurements in a Rotating Turbine Cooling Passage," Doctoral Thesis, Massachusetts Institute of Technology, Boston.
- Çakan, M., 2000, "Aero-Thermal Investigation of Fixed Rib-Roughened Internal Cooling Passages," Master of Science Thesis, Von Karman Institute for Fluid Dynamics.
- Guidez, J., 1989, "Study of the Convective Heat Transfer in a Rotating Coolant Channel," ASME, Journal of Turbomachinery, **111**, pp. 43-50.
- Han, J.C., Zhang, Y.M. and Lee, C.P., 1994, "Influence of Surface Heating Condition on Local Heat Transfer in a Rotating Square Channel with Smooth Walls and Radial Outward Flow," ASME, Journal of Turbomachinery, **116**, pp. 149-158.
- Hwang, G.J. and Kuo, C.R., 1994, "Experimental Study of Convective Heat Transfer in a Rotating Smooth Serpentine Passage with Radial Flow," ASME, HTD, **300**, pp. 139-146.
- Liou, T.M., Chen, M.Y. and Tsai, M.H., 2002, "Fluid Flow and Heat Transfer in a Rotating Two-Pass Square Duct with In-Line

90-deg Ribs," ASME, Journal of Turbomachinery, **124**, pp. 260-268.

Mochizuki, S., Takamura, J., Yamawaki, S. and Yang, W.J., 1994, "Heat Transfer in Serpentine Flow Passages with Rotation," ASME, Journal of Turbomachinery, **116**, pp. 133-140.

Servouze, Y., 1998, "3D Laser Anemometry in a Rotating Cooling Channel," ASME Turbo Expo98, Land, Sea & Air, Stockholm, Sweden, June 2-5, paper 98-GT-123.

Servouze, Y., Gicquel, P., Saccardi, E., Tanguy, B., Sauter, V., 1999, "3D Laser Anemometry in a Rotating Cooling Ribbed U-channel," IGTC '99 Kobe, Japan, November 14-19, paper F-059, pp. 849-855.

Taslim, M.E. and Wadsworth, C.M., 1997, "An Experimental Investigation of Rib Surface-Averaged Heat Transfer Coefficient in a Rib-Roughened Square Passage," ASME, Journal of Turbomachinery, **119**, pp. 381-389.